THE JOURNAL OF PHYSICAL CHEMISTRY LETTERS
A JOURNAL OF THE AMERICAN CHEMICAL SOCIETY

pubs.acs.org/JPCL

Letter

Single-Layer Dititanium Oxide Ti_2O MOene: Multifunctional Promises for Electride, Anode Materials, and Superconductor

Luo Yan, Tao Bo, Bao-Tian Wang, Sergei Tretiak, and Liujiang Zhou*

Cite This: *J. Phys. Chem. Lett.* 2021, 12, 494–500

Read Online

ACCESS | Metrics & More | Article Recommendations | Supporting Information

ABSTRACT: Using the first-principles calculations, we report the existence of the single-layer (SL) dititanium oxide Ti_2O (labeled as MOene) that constructs a novel family of MXene based on transition-metal oxides. This MOene material strongly contrasts the conventional ones consisting of transition-metal carbides and/or nitrides. SL Ti_2O has high thermal and dynamical stabilities because of the strong Ti−O ionic bonding interactions. Moreover, this material is an intrinsic electride and exhibits extremely low diffusion barriers of ∼12.0 and 6.3 meV for Li and Na diffusion, respectively. When applied as anode materials in lithium-ion batteries and sodium-ion batteries, it possesses a high energy storage capacity (960.23 $mAhg^{-1}$), surpassing the traditional MXenes-based anodes. The superb electrochemical performance stems from the existing anionic electron on Ti_2O surface. Astonishingly, SL Ti_2O is also determined to be a superconductor with a superconducting transition temperature (T_c) of ∼9.8 K, which originates from the soft-mode of the first acoustic phonon branch and enhanced electron−phonon coupling in the low-frequency region. Furthermore, this soft-mode behaves much softer upon applying a compressive strain of 2%, leading to a higher T_c of 11.9 K. Our finding broadens the family of MXenes and could facilitate more experimental efforts toward future nanodevices.

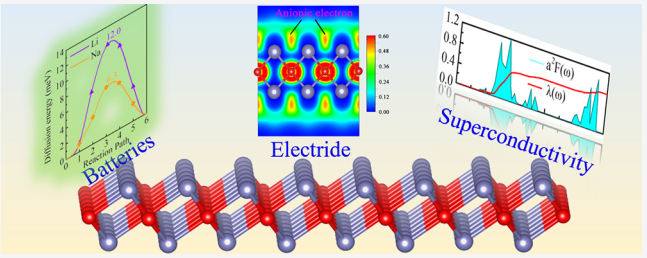

Recently, two-dimensional (2D) metal-shrouded crystals (MSC) (M_2X, M = metal and X = C, N) have triggered enormous interest because of their excellent mechanical and electronic (metallic and/or semiconducting) properties, providing promises for sensors,[1,2] catalysts,[3−5] energy storage,[6,7] (topological) electrides,[8,9] superconductors,[10−12] and so on. These MSC have a trigonal structure with two layers of M atoms covering one layer of X atoms. This family encompasses both nontransition and transition metal shrouded carbides or nitrides. The former includes alkali-metal and alkali-earth-metal carbides and nitrides (e.g., Ca_2N,[13] Mg_2C[14]), which were mainly investigated by theory. The latter refers to transition-metal shrouded MXenes (TMSM), including Ti_2C,[15] Mo_2C,[16] Ti_2N,[17] V_2C,[18] Nb_2C,[19] Y_2C,[8] and so on, which have been widely explored over the past few years.

Following remarkable promises of conventional MSM, metal-shrouded monochalcogenides, such as single-layer (SL) Tl_2O,[20] A_2X (A = Na, K, Rb, or Cs; X = O, S, Se, or Te),[21] KTlO,[22] and In_2X (X = O, S, Se),[23] have also showed fascinating physical and chemical traits, substantially enriching the family of 2D MSC. Considering the potential uses, the toxicity and scarcity of element Tl (as rare as gold) and the highly activity of alkali metals when exposed to ambient conditions seem to be detrimental. In contrast, Ti is a transition metal with a high abundance in the earth's crust[24] and multifarious uses in modern-day technologies. It is worthwhile to note that the bulk Ti_2O phase in a hexagonal lattice has been accessed in experiments since 1970,[25,26] motivating us to explore the existence of SL or few-layer Ti_2O with atomic thickness. Addressing this issue would not only open the door to a new family of MXenes (i.e., metal-shrouded 2D transition-metal oxides) but also potentially enrich the physics of 2D materials.

In this work, the first-principles calculations suggest that SL dititanium oxide Ti_2O is a novel family of MXene based on transition-metal oxides (labels as MOene to underline the 2D morphology) rather than conventional ones consisting of transition-metal carbides and/or nitrides. This MOene is a stable material and an intrinsic electride with anionic electron on the surface. The anionic states of 2D Ti_2O enable the very low diffusion barrier and large charge storage capacity when explored as an anode material of lithium-ion batteries (LIBs) and sodium-ion batteries (SIBs). Meanwhile, this MOene is a 2D superconductor with a T_c of ∼9.8 K. Such a combination of stability and exceptional electronic features implies a number of potential applications of Ti_2O in the next-generation nanodevices.

Received: November 14, 2020
Accepted: December 16, 2020
Published: December 29, 2020

https://dx.doi.org/10.1021/acs.jpclett.0c03397
J. Phys. Chem. Lett. 2021, 12, 494–500

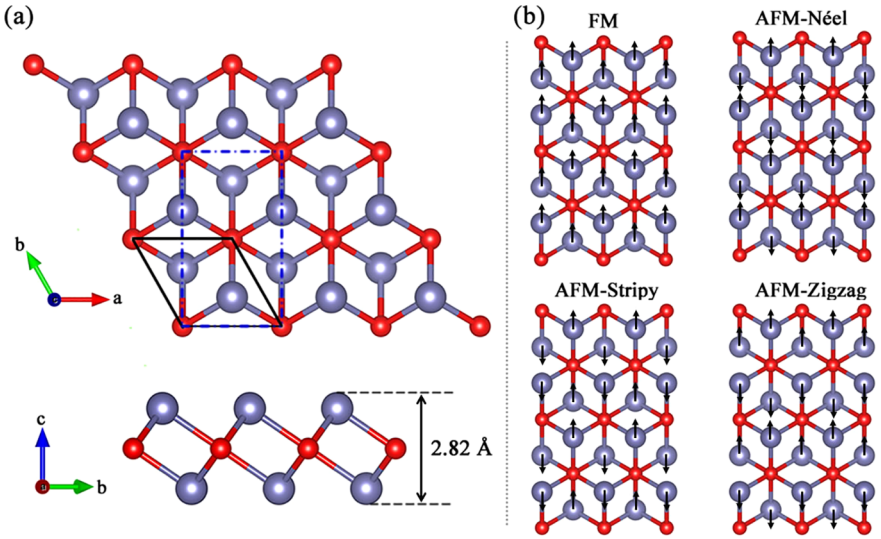

Figure 1. (a) Top (upper panel) and side (lower panel) views for SL Ti_2O. The rhombic primitive and conventional cells are labeled by black sold and blue dash lines, respectively. Silvery gray: Ti; red: O. (b) Four magnetic configurations of SL Ti_2O. The up and down arrows indicate spin-up and spin-down orientations, respectively.

Figure 1a shows the crystal model of SL Ti_2O. The SL structure optimizes in a hexagonal lattice with a space group $P\bar{3}m1$ (no. 164) and has a D_{3d} point symmetry. This structure is typical for SL MSM featuring the central oxygen octahedrally coordinated to six Ti atoms. Obviously, it breaks the traditional definition for MXenes, where X = C, N. Also, it is different from SL MBene, where X = B.[27] Here, we take SL Ti_2O as an example to propose a novel family of 2D material, MOene, where the O atomic layer is sandwiched by two transition-metal layers. To clearly determine its ground state, four types of spin-oriented configurations are considered (i.e., ferromagnetic (FM), antiferromagnetic Néel (AFM-Néel), antiferromagnetic Stripy (AFM-Stripy), and antiferromagnetic zigzag (AFM-Zigzag); Figure 1b). Their corresponding total energies and magnetic moments of each Ti atom are listed in 1.

Table 1. Total Energy (eV) of per Unit Cell and Magnetic Moment (μB) of per Ti Atom for Different Configurations of SL Ti_2O

configuration	energy (eV)	magnetic moment (μB)
nonmagnetic	−35.59192	0
FM	−35.59188	0
AFM-Néel	−35.83279	0.76
AFM-Stripy	−35.59192	0
AFM-Zigzag	−35.59191	0

Intriguingly, FM, AFM-Stripy, and AFM-Zigzag tend to be nonmagetic system with the same energy and zero magnetic moment on per Ti atoms. However, the AFM-Néel is the most stable configuration and has a magnetic moment 0.76 μ_B per Ti atom, arising from the dangling 3d orbitals of Ti atoms. Thus, the AFM-Néel configuration is used in the next simulations. The equilibrium lattice parameters are a = 2.82 Å, b = 4.88 Å, which is in accordance with experimental values of Ti_2O film (a = 2.84 Å).[28] The electron localization function (ELF) plot reveals the vanishing electron distributions between Ti and O atoms (Figure 2a), suggestive of the ionic-bonding interactions via which the charge transfer are from Ti to more electronegative O atoms (Figure S2a,b).

The dynamical stability of SL Ti_2O with AFM-Néel configuration is confirmed by the phonon spectrum lacking unstable modes (Figure S1a). The *ab initio* molecular dynamics (AIMD) simulations were carried out next to assess the thermal stability. SL Ti_2O is stable without Ti−O bonds breakage and geometric reconstructions up to 700 K (Figures S1b,c). The elastic constants are calculated to be $C_{11} = C_{22}$ = 133.7 N/m, C_{12} = 33.7 N/m, and C_{66} = 6.2 N/m, satisfying the mechanical stability criteria for a rectangle unit cell.[29,30] The in-plane Young's modulus ($Y_x = Y_y$) is 125.2 N/m. The Poisson's ratios along x and y directions (ν_x and ν_x) are both determined to be 0.25 due to the isotropic nature. The cohesive E_{coh} and formation E_f energies are 5.20 and −0.44 eV/atom, respectively, indicating its exothermic feature in the chemical synthesis and high experimental feasibility. Fortunately, the SL Ti_2O may be accessed via the chemical deposition on (0001)-oriented α-Al_2O_3 single crystalline substrate, as observed in Ti_2O thin films.[28]

Ti_2O monolayer is expected to accommodate the anionic states, as observed in other SL TMSM.[31−34] As shown in the ELF plot (Figure 2a), there are two excess electron pools localized above the SL Ti_2O surfaces as verified by the delocalized electride with anionic electrons. The chemical formula can thus be expressed as $[Ti_2O]^{2+} \cdot 2e^-$, similar to the Y_2C electride.[33] The difference charge plot shows the charges are mainly transferred from less-electronegative Ti to more electronegative O atoms and the center sites of anionic electrons (denoted as X pseudo atoms) that reside above the center of Ti atoms (Figure S2). The anionic electron bands (X-bands) are mostly located below the Fermi level (Figure 2b), in accordance with the partial density of states (PDOS) in the range of -3 eV $< E - E_F < 0$ eV (Figure 2c). Meanwhile, SL Ti_2O has a metallic feature with substantial electron states crossing the Fermi level. As indicated in Figure 2c, the dominant contributions to the electronic states near the Fermi level mainly stem from the hybridization between Ti-$d_{x^2-y^2,xy}$ and Ti-$d_{xz,yz}$ orbitals. The anionic electron sites have obvious hybridization with Ti-3d orbitals in the range of -3 eV $< E - E_F < 0$ eV (Figure 2b and Figures S3a,b). Therefore, anionic electrons are significantly from the unsaturated Ti-3d orbitals.

https://dx.doi.org/10.1021/acs.jpclett.0c03397
J. Phys. Chem. Lett. 2021, 12, 494−500

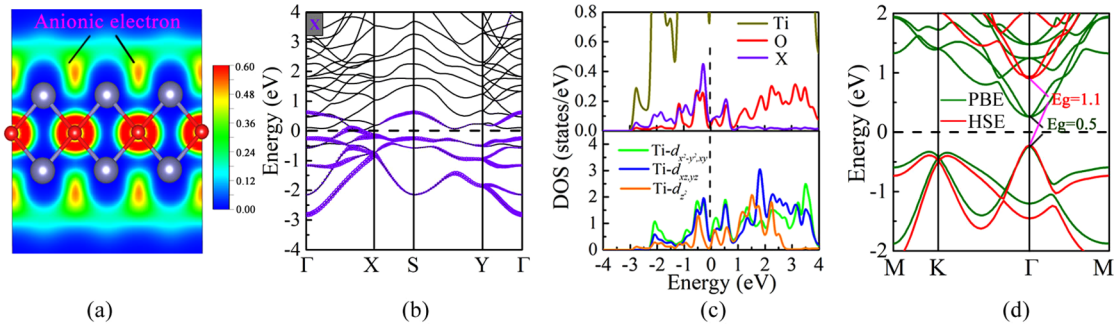

Figure 2. (a) The ELF slice of Ti_2O monolayer from $(0\bar{1}2)$ plane. The isovalue used is 0.4 au (b) The projected spin-up band structure with the anionic electrons highlighted in purple. (c) The spin-up PDOS of the Ti_2O monolayer. (d) The band structure of fluorinated SL Ti_2O within PBE and HSE. The Fermi levels are set to be zero.

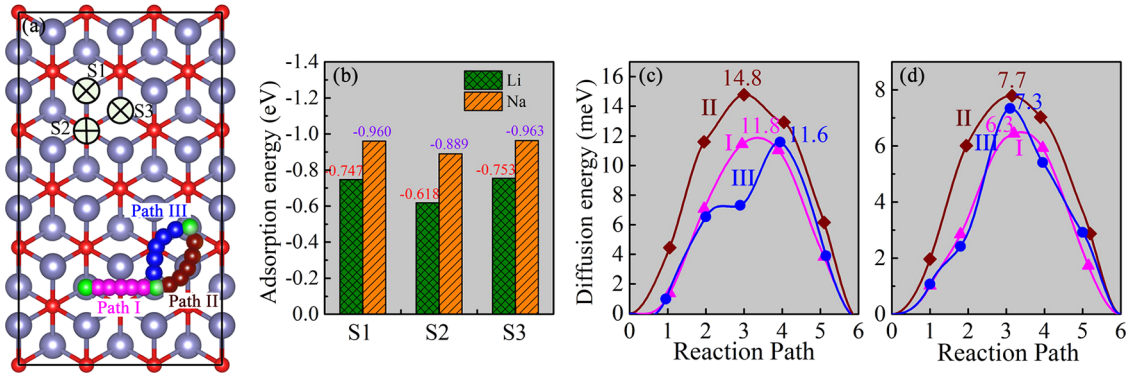

Figure 3. (a) The three Li/Na adsorption sites on Ti_2O monolayer: S1, S2 and S3. S1 and S2 are located on the top of Ti and O atoms, respectively; S3 is the hollow site of hexatomic ring consisting of Ti and O atoms. Three possible migration pathways I, II, III near the neighboring low-energy adsorption sites are marked. (b) The calculated adsorption energies of different sites on SL Ti_2O. The corresponding computed diffusion barriers of the (c) Li and (d) Na migration along path I, II, and III on Ti_2O monolayer, respectively.

To clearly determine the electronic states in the Ti_2O system, we further checked it in bulk Ti_2O. Intriguingly, the electronic states intrinsically reside within the interlayers (Figure S4), which helps to protect the electride states from oxygen or water contamination that destroys the anionic electride states of SL Ti_2O.

Since the electronic structures of conventional MXene are usually affected by surface functional groups, we here probe the functionalization on SL Ti_2O via fluoridation, hydrogenation, hydroxylation, and oxidization. Here, the four major possible functionalization configurations are considered (Figures S5,6). After full structure optimizations, the F and OH groups locating on the top of O atoms are most energetically favorable (Figure S5c), while the most stable configurations for H and O groups locate above the hollow site of hexatomic ring of Ti and O atoms (Figure S6b). All of the functionalized Ti_2O show a nonmagnetic ground state because the dangling 3d orbitals of the Ti atoms are saturated by corresponding functional groups. The phonon spectra confirm that the fluorinated, hydrogenated, hydroxylated SL Ti_2O are dynamically stable, while oxidized Ti_2O contains the unstable imaginary modes (Figure S7). The optimized lattice constants for Ti_2OF_2, Ti_2OH_2, and $Ti_2O(OH)_2$ are $a = b$ = 2.85, 2.83, and 2.89 Å, respectively. The band structures of Ti_2OF_2, Ti_2OH_2, and $Ti_2O(OH)_2$ are presented in Figures 2d and S8. Ti_2OH_2 and $Ti_2O(OH)_2$ are semimetal with finite electronic states crossing the Fermi level. In contrast, Ti_2OF_2 exhibits a semiconductor trait with a direct energy gap (E_g) of ~0.5 (PBE) and 1.1 eV (HSE) (Figure 2d), displaying great potentiality in optoelectronic devices. Thus, the electronic properties of SL Ti_2O can be efficiently tuned upon varying the surface functional groups.

Considering the promising application of conventional MXene materials in LIBs and SIBs,[35−39] we here explore the feasibility of Ti_2O MOene as a suitable electrode for the rechargeable batteries. The capability of energy storage for Ti_2O monolayer was investigated by the adsorption energies. Three typical Li/Na adsorption sites (labeled as S1−S3) were considered (Figure 3a). Calculated adsorption energies of Li/Na adsorption identified S3 site to be the most stable site with the lowest adsorption energies of being −0.75 and −0.96 eV for Li and Na atoms, respectively (Figure 2b). These adsorption energies are lower than those on Mo_2C (−0.58 eV for Li, − 0.77 eV for Na),[37] Ti_3C_2 (−0.50 eV for Li),[35] TiC_3 (−0.50 eV for Na),[38] and V_2C (−0.16 eV for Li)[36] and comparable to Ti_2N (−0.75 eV for Li, −0.95 eV for Na) monolayers,[39] indicating the strong interactions between the Li/Na atom and Ti_2O. Based on Bader analysis,[40] the net charge transfer from the adsorbed Li and Na atoms on the S3 site to the Ti_2O monolayer are 0.87 and 0.73 e/atom (Figure S9a,b), respectively, suggesting the ionic bonding feature stemming from the s−d hybridization between the Ti-3d and the metal s orbitals. Additionally, the Li and Na adsorbed systems maintain the metal trait (Figure S9c,d), indicating the good electronic conductivity in SL Ti_2O.

The charge−discharge rate was assessed via the energy barrier of Li/Na ion diffusion on Ti_2O monolayer using the climbing-image nudged elastic band (CI-NEB) method.[41] As shown in Figure 3c, the energy barrier for Li (Na) ion is low to

https://dx.doi.org/10.1021/acs.jpclett.0c03397
J. Phys. Chem. Lett. 2021, 12, 494−500

be about 12 (6.3) meV along the path I or III (I). The extremely low energy barrier indicates an ultrafast fast charge/discharge process when SL Ti_2O used as the anode materials. Such low diffusion barriers for Li and Na ions are lower than the previous values in other MXenes (~14−70 meV[35,37,39]), suggesting an ultraefficient Li/Na ion diffusion and thus ultrafast fast charge/discharge process on the SL Ti_2O when used in rechargeable batteries. This unprecedentedly small diffusion barrier can be attributed to the surface-confined anionic electrons, which helps to smooth the surface potential effectively, as confirmed in SL Ca_2N electride.[31]

Four configurations of Li/Na adducts (i.e., Ti_2OM_n(M = Li, Na), n = 1−4) (Figures S10a-d) on a 2 × 2 × 1 supercell were considered to evaluate the storage capacity via the concentration-dependent adsorption behaviors. All considered mixtures are energetically stable, confirmed by the negative formation energy and convex hulls (Figures 4a,c). Additionally,

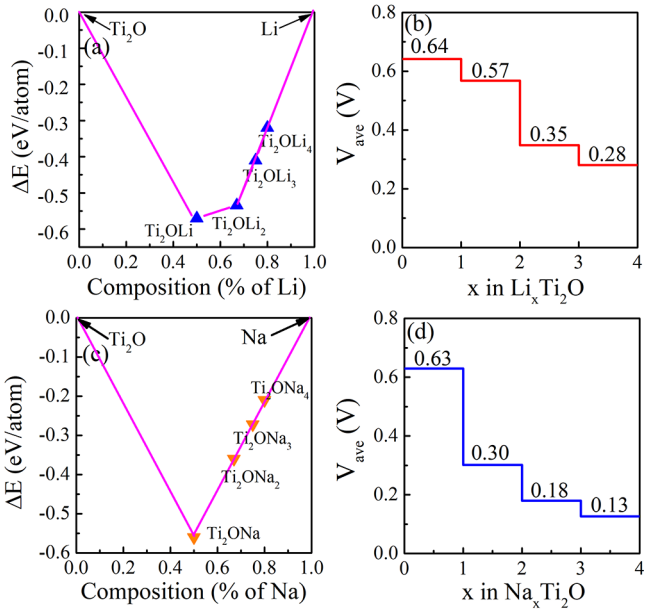

Figure 4. Hull of formation energies for the most stable configurations of (a) Li- and (c) Na-adsorbed Ti_2O monolayer. The OCV for each (b) Li and (d) Na concentration, respectively.

to estimate the volume effect, the geometries after full adsorption of Li and Na atoms are checked. The thicknesses of SL Ti_2O host after full adsorption of Li and Na atoms are 2.41 and 1.87 Å for the two-layer Li- and Na-adsorbed configurations, respectively. Compared with the pristine monolayer (2.82 Å), the volume of the fully Li (Na) adsorbed systems increases slightly to 2.73 (7.17) %. Meanwhile, the bond length of Ti−O has only a small change of ~1.4% for adsorbed mixtures. The layered E_{ave} are calculated to be −0.57 and −0.06 eV per atom for the one- and two-layer metal adsorption. Such a low absorption energy for the two-layer adatoms indicates a weak adsorption interactions. However, this value is still smaller than those of Mo_2C (−0.01 eV per atom)[37] and Nb_2C(−0.02 eV per atom)[42] and comparable to that V_2C (−0.06 eV per atom)[36] in LIBs. The layered E_{ave} for the one- and two-layer Na adatoms are −0.27 and −0.03 eV per atom. It should be worthy noted that the two-layer E_{ave} is still smaller than that of typical electrode materials in SIBs, such as MoN_2 (−0.02 eV per atom),[43] Ca_2N (−0.003 eV per atom),[31] and GeS (−0.02 eV per atom).[44] Therefore, the Li and Na atoms in the corresponding layer prefer to chemically bind to the host material (negative E_{ave}), rather than to form metal clusters (positive E_{ave}).[37,42,43] The theoretical capacities C_A for Ti_2O in LIBs and SIBs are 960.23 $mAhg^{-1}$, larger than those of conventional MXenes (100−542 $mAhg^{-1}$).[37,39,42,45] The ELF plots (Figure S11) upon Li and Na atoms adsorption reveal that the main origin of high capacity behavior is from the anionic electrons, which stabilize adsorbed Li/Na ions and favor the high adsorption concentration of Li/Na atoms.[46,47]

In addition, the average open-circuit voltage (OCV) in the range of 0−1.0 V indicates the ability to prevent the dendrite formation of alkali metals during the discharge/charge process.[38,39,48] There are four main plateaus during the Li (Na) insertion process (Figures 4b,d), showing a steady decreasing trend from 0.64 to 0.28 V (0.63 to 0.13 V) upon increasing the concentration of Li(Na) adatoms. Moreover, the OCV for full sodiations of Ti_2OLi_4 and Ti_2ONa_4 are 0.28 and 0.13 V, respectively, which are rather low and comparable to the typical anode materials in LIBs and SIBs, such as Mo_2C,[37] MoS_2,[49] TiC_3,[38] and Ti_3C_2[50], among others. Therefore, given the above discussions, the SL Ti_2O should be a excellent candidate as anode material for rechargeable LIBs and SIBs.

The superconductivity of the metallic SL Ti_2O was further investigated. Figure 5a shows the resolved phonon spectra in terms of the displacement directions of Ti and O atoms, in agreement with the projected phonon density of states (PhDOS) (Figure 5b). The out-of-plane modes of Ti atoms (Ti-z) dominate the low-frequency region (below 200 cm^{-1}). The mid-frequency region from 200 to 300 cm^{-1} mainly consists of in-plane vibrations of Ti atoms. Figure 5c shows

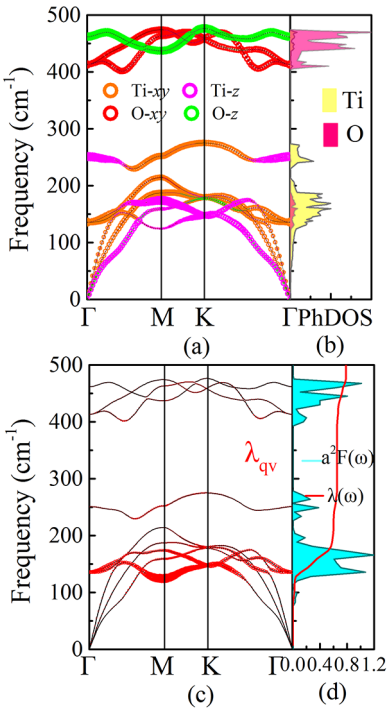

Figure 5. (a) The phonon spectra of Ti_2O resolved in terms of the vibration directions of Ti and O atoms. The orange, pink, red, and green hollow circles indicate Ti in-plane, Ti out-of-plane, O in-plane, and O out-of-plane modes, respectively. (b) PhDOS for Ti_2O. (c) The magnitude of the EPC λ_{qv}. (d) The Eliashberg spectral function $\alpha^2F(\omega)$ and the cumulative frequency-dependent EPC $\lambda(\omega)$.

https://dx.doi.org/10.1021/acs.jpclett.0c03397
J. Phys. Chem. Lett. 2021, 12, 494−500

that the relatively large strength of the electron−phonon coupling (EPC) (labeled by $\lambda_{q\nu}$) are related to the soft-modes in the first acoustic branch with a frequency of ∼150 cm^{-1}. This soft-mode that stems from the Ti-z vibrations makes a significant contribution to the cumulative frequency-dependent EPC function $\lambda(\omega)$. The Eliashberg spectral function α^2F reveals that the two major peaks in the low frequency region of 100−200 cm^{-1} lead to a rapid increase of the cumulative $\lambda(\omega)$ (Figure 5d), evidencing the jump of the total EPC in this range and pointing to a medium-coupling superconductor with a λ = 0.72. Based on the McMillian−Allen−Dynes formula,[51] the superconducting transition temperature T_c is evaluated to be ∼9.8 K, higher than or comparable to that of MXene-based superconductors [Mo_2C (3.0 K),[10,11] Ti_2C (1.3 K)[11] and functioned Nb_2C (4.5−7.1 K).[52]] and 2D boride-based superconductors [B allotrope (6.7 K),[53] Mo_2B_2 (3.9 K),[54] W_2B_2 (7.8 K),[55] AlB_6 (0.95 K),[56] GaB_6 (1.7 K), InB_6 (7.8 K),[57] Li_2B_7,[58] and B_2O (10.35 K).[59] Besides, the T_c is associated with screened Coulomb repulsion constant (μ^*). As shown in Figure S12a, the T_c decreases monotonically from 11.4 to 6.3 K upon the increase of μ^* from 0.08 to 0.15. The superconductivity of Ti_2O monolayer when subject to external strains were also investigated so as to describe the strain effects from substrates in the process of chemical deposition. Clearly, the tensile strains weaken the soft-mode vibrations of the first acoustic branch around the M point, thus producing a weaker EPC (Figure S12b). On the contrary, the compressive strains would enhance the EPC verified by a much softer mode at the M point (Figure S12b). The maximum value of T_c of 11.9 K is achieved at a compressive strain of 2% (Figure S12c). All in all, this superconductivity in Ti_2O MOene enriches the 2D MXene-based superconductors that are only observed in Mo_2C, Ti_2C, and Nb_2C materials.[10,11,52]

In summary, we report a systematically theoretical investigation of a new SL metal-shrouded MOene, namely 2D dititanium oxide Ti_2O, in great contrast conventional MXenes that consists of transition-metal carbides and/or nitrides. This thermally and dynamically stable MOene is an electride in monolayer and bulk form. Ti_2O MOene can be used as an anode material in lithium and sodium battery technologies, owing to extremely low diffusion barriers (12.0 meV for LIBs and 6.3 meV for NIBs) and an excellent storage capacity (960.23 $mAhg^{-1}$). The anionic electrons intercalating the adsorbed Li/Na atoms and Ti_2O monolayer make the significant contributions to the very fast charge/discharge process. Moreover, within the Bardeen−Cooper−Schrieffer microscopic theory,[60−63] Ti_2O is determined to be a intrinsic superconductor with a transition temperature T_c of 9.8 K. The superconductivity mainly originates from the presence of soft modes in the first acoustic branch and a significant enhancement of EPC in the low-frequency region. The T_c could reach a maximum value of 11.9 K when subject to a compressive strain of 2%. These results endow Ti_2O MOene with multifunctionality, promisingly suitable for future nanodevices and energy storage technologies and thus call for further experimental fabrication and characterization efforts.

First-principles calculations based on the density functional theory (DFT) calculations were performed according to the projector augmented wave (PAW) scheme. The exchange and correlation contributions were simulated within the generalized gradient approximation (GGA)[64,65] as formulated by Perdew−Burke−Ernzerhof (PBE).[66] A rapid dispersion-corrected DFT method (opt88-vdw) was adopted to model the van der Waals interaction.[67] A subset of numerically expensive calculations were performed with an accurate screened exchange hybrid density functional by HSE06[68] and inclusion of spin−orbit coupling (SOC) terms. The plane-wave cutoff energy of 550 eV and Γ-centered 21 × 21 × 1 k-point mesh using the Monkhorst−Pack method were adopted in electronic structure calculations. To avoid the interactions between the nearest-neighbor unit cells, a vacuum thickness of 20 Å along the z direction was applied. The geometry optimizations were carried out with a convergence threshold of 10^{-5} eV in total energy and of 0.01 eV $Å^{-1}$ in maximum force per each atom. Some data analyses were done with the help of VASPKIT.[69] See more details in Supporting Information.

■ ASSOCIATED CONTENT

Supporting Information

The Supporting Information is available free of charge at https://pubs.acs.org/doi/10.1021/acs.jpclett.0c03397.

Detail methods; phonon spectrum; AIMD simulations; difference charge density; projected band structures; ELF plot of bulk Ti_2O; configurations and phonon spectra for fluorinated, hydrogenated, oxidized and hydroxylated SL Ti_2O; the most stable configurations with different Li/Na concentrations in Ti_2OM_n(M = Li,Na) (n = 1−4); ELF plots for the Li/Na atoms adsorbed Ti_2O monolayer; the changes of T_c under the variable μ^*; and variations of phonon spectra, λ, and T_c under biaxial strains (PDF)

■ AUTHOR INFORMATION

Corresponding Author

Liujiang Zhou − *Institute of Fundamental and Frontier Sciences, University of Electronic Science and Technology of China, Chengdu 610054, P. R. China;* orcid.org/0000-0001-5814-4486; Email: liujiang86@gmail.com

Authors

Luo Yan − *Institute of Fundamental and Frontier Sciences, University of Electronic Science and Technology of China, Chengdu 610054, P. R. China;* orcid.org/0000-0002-3563-0489

Tao Bo − *Songshan Lake Materials Laboratory, Dongguan, Guangdong 523808, China*

Bao-Tian Wang − *Spallation Neutron Source Science Center, Institute of High Energy Physics, Chinese Academy of Sciences, Dongguan 523803, China; Collaborative Innovation Center of Extreme Optics, Shanxi University, Taiyuan, Shanxi 030006, China;* orcid.org/0000-0002-4032-3344

Sergei Tretiak − *Theoretical Physics and Chemistry of Materials, Los Alamos National Laboratory, Los Alamos, New Mexico 87545, United States; Skolkovo Institute of Science and Technology, Moscow 143026, Russia;* orcid.org/0000-0001-5547-3647

Complete contact information is available at: https://pubs.acs.org/10.1021/acs.jpclett.0c03397

Notes

The authors declare no competing financial interest.

https://dx.doi.org/10.1021/acs.jpclett.0c03397
J. Phys. Chem. Lett. 2021, 12, 494−500

■ ACKNOWLEDGMENTS

L.Z. acknowledges the financial support from the University of Electronic Science and Technology of China. This work was performed in part at the Center for Integrated Nanotechnology (CINT), a U.S. Department of Energy and Office of Basic Energy Sciences user facility. B.-T.W. acknowledge financial support from the Natural Science Foundation of China (Grants No. 11675195 and No. 12074381). S.T. acknowledges support from the Los Alamos National Laboratory (LANL) Directed Research and Development funds (LDRD).

■ REFERENCES

(1) Liu, H.; Duan, C.; Yang, C.; Shen, W.; Wang, F.; Zhu, Z. A novel nitrite biosensor based on the direct electrochemistry of hemoglobin immobilized on MXene-Ti_3C_2. *Sens. Actuators, B* **2015**, *218*, 60−66.
(2) Yu, X.-f.; Li, Y.-c.; Cheng, J.-b.; Liu, Z.-b.; Li, Q.-z.; Li, W.-z.; Yang, X.; Xiao, B. Monolayer Ti_2CO_2: A promising candidate for NH_3 sensor or capturer with high sensitivity and selectivity. *ACS Appl. Mater. Interfaces* **2015**, *7*, 13707−13713.
(3) Gao, Y.; Wang, L.; Li, Z.; Zhou, A.; Hu, Q.; Cao, X. Preparation of MXene-Cu_2O nanocomposite and effect on thermal decomposition of ammonium perchlorate. *Solid State Sci.* **2014**, *35*, 62−65.
(4) Seh, Z. W.; Fredrickson, K. D.; Anasori, B.; Kibsgaard, J.; Strickler, A. L.; Lukatskaya, M. R.; Gogotsi, Y.; Jaramillo, T. F.; Vojvodic, A. Two-dimensional molybdenum carbide (MXene) as an efficient electrocatalyst for hydrogen evolution. *ACS Energy Lett.* **2016**, *1*, 589−594.
(5) Xiong, D.; Li, X.; Bai, Z.; Lu, S. Recent advances in layered $Ti_3C_2T_x$ MXene for electrochemical energy storage. *Small* **2018**, *14*, 1703419.
(6) Anasori, B.; Lukatskaya, M. R.; Gogotsi, Y. 2D metal carbides and nitrides (MXenes) for energy storage. *Nat. Rev. Mater.* **2017**, *2*, 1−17.
(7) Sun, S.; Liao, C.; Hafez, A. M.; Zhu, H.; Wu, S. Two-dimensional MXenes for energy storage. *Chem. Eng. J.* **2018**, *338*, 27−45.
(8) Huang, H.; Jin, K.-H.; Zhang, S.; Liu, F. Topological Electride Y_2C. *Nano Lett.* **2018**, *18*, 1972−1977.
(9) Zhou, L.; Zhang, Y.; Zhuo, Z.; Neukirch, A. J.; Tretiak, S. Interlayer-decoupled Sc-based Mxene with high carrier mobility and strong light-harvesting ability. *J. Phys. Chem. Lett.* **2018**, *9*, 6915−6920.
(10) Xu, C.; Wang, L.; Liu, Z.; Chen, L.; Guo, J.; Kang, N.; Ma, X.-L.; Cheng, H.-M.; Ren, W. Large-area high-quality 2D ultrathin Mo_2C superconducting crystals. *Nat. Mater.* **2015**, *14*, 1135−1141.
(11) Lei, J.; Kutana, A.; Yakobson, B. I. Predicting stable phase monolayer Mo_2C (MXene), a superconductor with chemically-tunable critical temperature. *J. Mater. Chem. C* **2017**, *5*, 3438−3444.
(12) Zhang, J.-J.; Dong, S. Superconductivity of monolayer Mo_2C: The key role of functional groups. *J. Chem. Phys.* **2017**, *146*, 034705.
(13) Zhao, S.; Li, Z.; Yang, J. Obtaining two-dimensional electron gas in free space without resorting to electron doping: an electride based design. *J. Am. Chem. Soc.* **2014**, *136*, 13313−13318.
(14) Wang, S.-S.; Liu, Y.; Yu, Z.-M.; Sheng, X.-L.; Zhu, L.; Guan, S.; Yang, S. A. Monolayer Mg_2C: Negative poisson's ratio and unconventional two-dimensional emergent fermions. *Phys. Rev. Mater.* **2018**, *2*, 104003.
(15) Naguib, M.; Mashtalir, O.; Carle, J.; Presser, V.; Lu, J.; Hultman, L.; Gogotsi, Y.; Barsoum, M. W. Two-dimensional transition metal carbides. *ACS Nano* **2012**, *6*, 1322−1331.
(16) Meshkian, R.; Näslund, L.-Å.; Halim, J.; Lu, J.; Barsoum, M. W.; Rosen, J. Synthesis of two-dimensional molybdenum carbide, Mo_2C, from the gallium based atomic laminate Mo_2Ga_2C. *Scr. Mater.* **2015**, *108*, 147−150.
(17) Soundiraraju, B.; George, B. K. Two-dimensional titanium nitride (Ti_2N) MXene: Synthesis, characterization, and potential application as surface-enhanced raman scattering substrate. *ACS Nano* **2017**, *11*, 8892−8900.
(18) Liu, F.; Zhou, J.; Wang, S.; Wang, B.; Shen, C.; Wang, L.; Hu, Q.; Huang, Q.; Zhou, A. Preparation of high-purity V_2C MXene and electrochemical properties as Li-ion batteries. *J. Electrochem. Soc.* **2017**, *164*, A709−A713.
(19) Naguib, M.; Halim, J.; Lu, J.; Cook, K. M.; Hultman, L.; Gogotsi, Y.; Barsoum, M. W. New two-dimensional niobium and vanadium carbides as promising materials for Li-ion batteries. *J. Am. Chem. Soc.* **2013**, *135*, 15966−15969.
(20) Ma, Y.; Kuc, A.; Heine, T. Single-Layer Tl_2O: A metal-shrouded 2D semiconductor with high electronic mobility. *J. Am. Chem. Soc.* **2017**, *139*, 11694−11697.
(21) Hua, C.; Sheng, F.; Hu, Q.; Xu, Z.-A.; Lu, Y.; Zheng, Y. Dialkali-metal monochalcogenide semiconductors with high mobility and tunable magnetism. *J. Phys. Chem. Lett.* **2018**, *9*, 6695−6701.
(22) Song, Y.; Yuan, J.; Li, L.; Xu, M.; Wang, J.; Xue, K.; Miao, X. KTlO: A metal shrouded 2D semiconductor with high carrier mobility and tunable magnetism. *Nanoscale* **2019**, *11*, 1131−1139.
(23) Li, H.; Hu, S.; Zhao, S.; Lan, C. First-principles study on the electronic and optical properties of 2D chalcogenides M_2X and M_2X_3 (M = Tl, In and X = O, S, Se). *Chem. Phys. Lett.* **2020**, *749*, 137404.
(24) Tan, L.; Chi-lung, Y. Abundance of chemical elements in the earth's crust and its major tectonic units. *Int. Geol. Rev.* **1970**, *12*, 778−786.
(25) Kornilov, I. I.; Vavilova, V. V.; Fykin, L. E.; Ozerov, R. P.; Solowiev, S. P.; Smirnov, V. P. Neutron diffraction investigation of ordered structures in the titanium-oxygen system. *Metall. Mater. Trans. B* **1970**, *1*, 2569.
(26) Novoselova, T.; Malinov, S.; Sha, W.; Zhecheva, A. High-temperature synchrotron x-ray diffraction study of phases in a gamma TiAl alloy. *Mater. Sci. Eng., A* **2004**, *371*, 103−112.
(27) Ozdemir, I.; Kadioglu, Y.; Akturk, O. U.; Yuksel, Y.; Akinci, U.; Akturk, E. A new single-layer structure of MBene family: Ti_2B. *J. Phys.: Condens. Matter* **2019**, *31*, 505401.
(28) Fan, Y.; Zhang, C.; Liu, X.; Lin, Y.; Gao, G.; Ma, C.; Yin, Y.; Li, X. Structure and transport properties of titanium oxide (Ti_2O, $TiO_{1+\delta}$, and Ti_3O_5) thin films. *J. Alloys Compd.* **2019**, *786*, 607−613.
(29) Born, M.; Huang, K. *Dynamical theory of crystal lattices*; Clarendon Press, 1954.
(30) Mouhat, F.; Coudert, F.-X. Necessary and sufficient elastic stability conditions in various crystal systems. *Phys. Rev. B: Condens. Matter Mater. Phys.* **2014**, *90*, 224104.
(31) Hu, J.; Xu, B.; Yang, S. A.; Guan, S.; Ouyang, C.; Yao, Y. 2D electrides as promising anode materials for Na-ion batteries from first-principles study. *ACS Appl. Mater. Interfaces* **2015**, *7*, 24016−24022.
(32) Lee, K.; Kim, S. W.; Toda, Y.; Matsuishi, S.; Hosono, H. Dicalcium nitride as a two-dimensional electride with an anionic electron layer. *Nature* **2013**, *494*, 336−340.
(33) Park, J.; Lee, K.; Lee, S. Y.; Nandadasa, C.; Kim, S.; Lee, K. H.; Lee, Y. H.; Hosono, H.; Kim, S.; Kim, S. W. Strong localization of anionic electrons at interlayer for electrical and magnetic anisotropy in two-dimensional Y_2C electride. *J. Am. Chem. Soc.* **2017**, *139*, 615−618.
(34) Zhou, L.; Zhang, Y.; Zhuo, Z.; Neukirch, A. J.; Tretiak, S. Interlayer-decoupled Sc-based Mxene with high carrier mobility and strong light-harvesting ability. *J. Phys. Chem. Lett.* **2018**, *9*, 6915−6920.
(35) Tang, Q.; Zhou, Z.; Shen, P. Are MXenes promising anode materials for Li ion batteries? Computational studies on electronic properties and Li storage capability of Ti_3C_2 and $Ti_3C_2X_2$ (X= F, OH) monolayer. *J. Am. Chem. Soc.* **2012**, *134*, 16909−16916.
(36) Hu, J.; Xu, B.; Ouyang, C.; Yang, S. A.; Yao, Y. Investigations on V_2C and V_2CX_2 (X= F, OH) monolayer as a promising anode material for Li ion batteries from first-principles calculations. *J. Phys. Chem. C* **2014**, *118*, 24274−24281.
(37) Sun, Q.; Dai, Y.; Ma, Y.; Jing, T.; Wei, W.; Huang, B. Ab initio prediction and characterization of Mo_2C monolayer as anodes for

https://dx.doi.org/10.1021/acs.jpclett.0c03397
J. Phys. Chem. Lett. 2021, 12, 494−500

lithium-ion and sodium-ion batteries. *J. Phys. Chem. Lett.* **2016**, *7*, 937−943.
(38) Yu, T.; Zhao, Z.; Liu, L.; Zhang, S.; Xu, H.; Yang, G. TiC_3 monolayer with high specific capacity for sodium-ion batteries. *J. Am. Chem. Soc.* **2018**, *140*, 5962−5968.
(39) Wang, D.; Gao, Y.; Liu, Y.; Jin, D.; Gogotsi, Y.; Meng, X.; Du, F.; Chen, G.; Wei, Y. First-principles calculations of Ti_2N and Ti_2NT_2 (T= O, F, OH) monolayers as potential anode materials for lithium-ion batteries and beyond. *J. Phys. Chem. C* **2017**, *121*, 13025−13034.
(40) Tang, W.; Sanville, E.; Henkelman, G. A grid-based bader analysis algorithm without lattice bias. *J. Phys.: Condens. Matter* **2009**, *21*, 084204−084204.
(41) Mills, G.; Jónsson, H. Quantum and thermal effects in H_2 dissociative adsorption: evaluation of free energy barriers in multidimensional quantum systems. *Phys. Rev. Lett.* **1994**, *72*, 1124.
(42) Hu, J.; Xu, B.; Ouyang, C.; Zhang, Y.; Yang, S. A. Investigations on Nb_2C monolayer as promising anode material for Li or non-Li ion batteries from first-principles calculations. *RSC Adv.* **2016**, *6*, 27467−27474.
(43) Zhang, X.; Yu, Z.; Wang, S.-S.; Guan, S.; Yang, H. Y.; Yao, Y.; Yang, S. A. Theoretical prediction of MoN_2 monolayer as a high capacity electrode material for metal ion batteries. *J. Mater. Chem. A* **2016**, *4*, 15224−15231.
(44) Li, F.; Qu, Y.; Zhao, M. Germanium sulfide nanosheet: A universal anode material for alkali metal ion batteries. *J. Mater. Chem. A* **2016**, *4*, 8905−8912.
(45) Xie, Y.; Naguib, M.; Mochalin, V. N.; Barsoum, M. W.; Gogotsi, Y.; Yu, X.; Nam, K.-W.; Yang, X.-Q.; Kolesnikov, A. I.; Kent, P. R. Role of surface structure on Li-ion energy storage capacity of two-dimensional transition-metal carbides. *J. Am. Chem. Soc.* **2014**, *136*, 6385−6394.
(46) Xie, Y.; Dall'Agnese, Y.; Naguib, M.; Gogotsi, Y.; Barsoum, M. W.; Zhuang, H. L.; Kent, P. R. Prediction and characterization of MXene nanosheet anodes for non-lithium-ion batteries. *ACS Nano* **2014**, *8*, 9606−9615.
(47) Xu, J.; Wang, D.; Lian, R.; Gao, X.; Liu, Y.; Yury, G.; Chen, G.; Wei, Y. Structural prediction and multilayer Li^+ storage in two-dimensional VC_2 carbide studied by first-principles calculations. *J. Mater. Chem. A* **2019**, *7*, 8873−8881.
(48) Eames, C.; Islam, M. S. Ion intercalation into two-dimensional transition-metal carbides: global screening for new high-capacity battery materials. *J. Am. Chem. Soc.* **2014**, *136*, 16270−16276.
(49) Hu, Z.; Wang, L.; Zhang, K.; Wang, J.; Cheng, F.; Tao, Z.; Chen, J. MoS_2 nanoflowers with expanded interlayers as high-performance anodes for sodium-ion batteries. *Angew. Chem., Int. Ed.* **2014**, *53*, 12794−12798.
(50) Er, D.; Li, J.; Naguib, M.; Gogotsi, Y.; Shenoy, V. B. Ti_3C_2 MXene as a high capacity electrode material for metal (Li, Na, K, Ca) ion batteries. *ACS Appl. Mater. Interfaces* **2014**, *6*, 11173−11179.
(51) Allen, P. B.; Dynes, R. Transition temperature of strong-coupled superconductors reanalyzed. *Phys. Rev. B* **1975**, *12*, 905.
(52) Kamysbayev, V.; Filatov, A. S.; Hu, H.; Rui, X.; Lagunas, F.; Wang, D.; Klie, R. F.; Talapin, D. V. Covalent surface modifications and superconductivity of two-dimensional metal carbide MXenes. *Science* **2020**, *369*, 979−983.
(53) Zhao, Y.; Zeng, S.; Ni, J. Superconductivity in two-dimensional boron allotropes. *Phys. Rev. B: Condens. Matter Mater. Phys.* **2016**, *93*, 014502.
(54) Yan, L.; Bo, T.; Liu, P.-F.; Wang, B.-T.; Xiao, Y.-G.; Tang, M.-H. Prediction of phonon-mediated superconductivity in two-dimensional Mo_2B_2. *J. Mater. Chem. C* **2019**, *7*, 2589−2595.
(55) Yan, L.; Bo, T.; Zhang, W.-X.; Liu, P.-F.; Lu, Z.-S.; Xiao, Y.-G.; Tang, M.-H.; Wang, B.-T. Novel structures of two-dimensional tungsten boride and their superconductivity. *Phys. Chem. Chem. Phys.* **2019**, *21*, 15327−15338.
(56) Song, B.; Zhou, Y.; Yang, H.-M.; Liao, J.-H.; Yang, L.-M.; Yang, X.-B.; Ganz, E. Two-dimensional anti-van't Hoff/Le Bel array AlB_6 with high stability, unique motif, triple dirac cones and superconductivity. *J. Am. Chem. Soc.* **2019**, *141*, 3630−3640.
(57) Yan, L.; Bo, T.; Liu, P.-F.; Zhou, L.; Zhang, J.; Tang, M.; Xiao, Y.; Wang, B. Superconductivity in predicted two dimensional XB_6 (X= Ga, In). *J. Mater. Chem. C* **2020**, *8*, 1704−1714.
(58) Wu, C.; Wang, H.; Zhang, J.; Gou, G.; Pan, B.; Li, J. Lithium−boron (Li−B) monolayers: First-principles cluster expansion and possible two-dimensional superconductivity. *ACS Appl. Mater. Interfaces* **2016**, *8*, 2526−2532.
(59) Yan, L.; Liu, P.-F.; Li, H.; Tang, Y.; He, J.; Huang, X.; Wang, B.-T.; Zhou, L. Theoretical dissection of superconductivity in two-dimensional honeycomb borophene oxide B_2O crystal with a high stability. *NPJ. Comput. Mater.* **2020**, *6*, 1−7.
(60) Bardeen, J.; Cooper, L. N.; Schrieffer, J. R. Theory of superconductivity. *Phys. Rev.* **1957**, *108*, 1175.
(61) Zhang, X.; Zhou, Y.; Cui, B.; Zhao, M.; Liu, F. Theoretical discovery of a superconducting two-dimensional metal−organic framework. *Nano Lett.* **2017**, *17*, 6166−6170.
(62) Grimvall, G. *The electron-phonon interaction in metals*; North-Holland Amsterdam, 1981; Vol. *8*.
(63) Giustino, F. Electron-phonon interactions from first principles. *Rev. Mod. Phys.* **2017**, *89*, 015003.
(64) Blöchl, P. E. Projector augmented-wave method. *Phys. Rev. B: Condens. Matter Mater. Phys.* **1994**, *50*, 17953.
(65) Blöchl, P. E.; Jepsen, O.; Andersen, O. K. Improved tetrahedron method for brillouin-zone integrations. *Phys. Rev. B: Condens. Matter Mater. Phys.* **1994**, *49*, 16223.
(66) Perdew, J. P.; Burke, K.; Ernzerhof, M. Generalized gradient approximation made simple. *Phys. Rev. Lett.* **1996**, *77*, 3865.
(67) Klimes, J.; Bowler, D. R.; Michaelides, A. Van der waals density functionals applied to solids. *Phys. Rev. B: Condens. Matter Mater. Phys.* **2011**, *83*, 195131.
(68) Heyd, J.; Scuseria, G. E. Efficient hybrid density functional calculations in solids: Assessment of the heyd-scuseria-ernzerhof screened coulomb hybrid functional. *J. Chem. Phys.* **2004**, *121*, 1187−1192.
(69) Wang, V.; Xu, N.; Liu, J. C.; Tang, G.; Geng, W.-T. Vaspkit: A user-friendly interface facilitating high-throughput computing and analysis using vasp code. *arXiv (Materials Science)*, Aug. 22, **2019**, 1908.08269. https://arxiv.org/abs/1908.08269.

https://dx.doi.org/10.1021/acs.jpclett.0c03397
J. Phys. Chem. Lett. 2021, 12, 494−500